PHILOSOPHICAL TRANSACTIONS OF THE ROYAL SOCIETY A MATHEMATICAL, PHYSICAL & ENGINEERING SCIENCES

Acoustic cavitation: the fluid dynamics of non–spherical bubbles

John R. Blake, Giles S. Keen, Robert P. Tong and Miles Wilson

Phil. Trans. R. Soc. Lond. A 1999 **357**, 251-267
doi: 10.1098/rsta.1999.0326

THE ROYAL SOCIETY

Acoustic cavitation: the fluid dynamics of non-spherical bubbles

By John R. Blake, Giles S. Keen, Robert P. Tong and Miles Wilson

School of Mathematics and Statistics, University of Birmingham, Edgbaston, Birmingham B15 2TT, UK

In acoustic cavitation the spatial variation and time-dependent nature of the acoustic pressure field, whether it is a standing or propagating wave, together with the presence of other bubbles, particles and boundaries produces gradients and asymmetries in the flow field. This will inevitably lead to non-spherical bubble behaviour, often of short duration, before break-up into smaller bubbles which may act as nuclei for the generation of further bubbles. During the collapse phase, high temperatures and pressures will occur in the gaseous interior of the bubble.

This paper concentrates on the non-spherical bubble extension to the earlier spherical-bubble studies for acoustic cavitation by exploiting the techniques that had previously been used to model incompressible hydraulic cavitation phenomena. Bubble behaviour near an oscillating boundary, jet impact and damage to boundaries, bubble interactions, bubble clouds and bubble behaviour near rough surfaces are considered. In many cases the key manifestation of the asymmetry is the development of a high-speed liquid jet that penetrates the interior of the bubble. Jetting behaviour can lead to high pressures, high strain rates (of importance to break-up of macromolecules) and toroidal bubbles, all of which can enhance mixing. In addition it may provide a mechanism for injecting the liquid into the hot bubble interior. Many practical applications such as cleaning, enhanced rates of chemical reactions, luminescence and novel metallurgical processes may be associated with this phenomenon.

Keywords: acoustic cavitation; non-spherical bubbles; liquid jet; toroidal bubble; sonoluminescence

1. Introduction

Acoustic cavitation is one of the exciting areas of research in contemporary physics and chemistry, with the potential to provide solutions to a range of chemical, metallurgical and environmental problems caused by the enormous pressures and temperatures that can be generated inside the cavitation bubbles. The modelling of these phenomena is extremely complex, not only because of the 'unknown' bubble shape but also because the fluid mechanics of the compressible liquid outside and the internal gas dynamics need to be modelled accurately. To date, many theoretical studies have concentrated on spherical bubbles with the potential for development of a spherical shock wave inside the collapsing bubble. However, it is unlikely that most bubbles will remain spherical, with recent examples being illustrated by the studies of Ohl *et al*. (this issue) for laser-generated bubbles near boundaries and the earlier doubts expressed by Prosperetti (1997) concerning the mechanism for light

generation in single-bubble sonoluminescence (although see Prosperetti & Hao (this issue) and Ohl *et al*. (this issue)).

Non-spherical bubbles require the solution of partial differential equations, either Laplace's equation for effectively incompressible flows, or the wave equation for weakly compressible flows. Indeed, as the radius of the bubble R_0 is often much smaller than the acoustic wavelength λ (i.e. $R_0/\lambda \ll 1$), there is effectively an 'inner' region around the bubble which may be regarded as incompressible. These ideas were exploited by Prosperetti (1984) and others in earlier models of acoustic cavitation and the derivation of the weakly compressible spherical-bubble equations (Keller & Kolodner 1956; Gilmore 1952). Current studies are extending the approach of Prosperetti (1984) to non-spherical bubbles. For high-amplitude acoustic driving pressures the full equations need to be solved (Moss *et al*. 1994). This paper will concentrate primarily on the knowledge that can be gained from incompressible-flow studies that have, for the most part, concentrated on laboratory studies of the growth and collapse of vapour cavities normally generated by a spark discharge or a laser (where luminescence is generated in these studies, it is known as 'single-cavitation bubble luminescence' (SCBL)) (Ohl *et al*. 1998, this issue; Lohse 1998).

2. Acoustic pressure fields, acoustic streaming and microstreaming

Before developing the theoretical models, it is worthwhile briefly commenting on three phenomena, namely acoustic pressure fields, acoustic streaming and microstreaming. At the linear approximation of the fluid-mechanics equations the determination of the flow field involves the solution of the wave equation, characterized by the speed of sound which, for a given driving frequency, determines the wavelength of the acoustic wave. Clearly the source of sound from a specific device is often located over a finite area, and complicated pressure and velocity fields can result. An excellent review of this topic may be found in Leighton (1994). This aspect of real situations will be simplified in the theory presented in this paper for the pressure field around a minute bubble. For the most part we will be considering periodic pressure fields or impulse-type flow fields obtained by using either a spark (see, for example, Blake & Gibson 1987; Tomita & Shima 1986) or laser discharge (see Ohl *et al*. this issue; Tomita & Shima 1986). This approach is often used to study the behaviour of short-lifetime cavitation bubbles near different surfaces and has applications in laser surgery and extracorporeal shock-wave lithotripsy (ESWL).

A particle or a bubble in an acoustic pressure field will translate and thence experience a small change in the pressure and velocity field, leading to a Lagrangian drift of the particle. However, velocities associated with drift are small compared to observed motions near an ultrasonic horn, hence other mechanisms need to be considered. The important contribution comes from the so-called Reynolds stress, terms arising from the nonlinear momentum terms in the Navier–Stokes equations (Lighthill 1978*a*, *b*; Riley 1998). Often due to various attenuation mechanisms, a gradient of the Reynolds stresses exists leading to a force per unit volume acting on the fluid. For high Reynolds numbers this leads to a 'round jet', observed as the 'quartz wind', while for low values recirculating 'stokeslet' eddies can exist near a boundary (Blake 1971; Lighthill 1978*a*, *b*). This environment can lead to a vigorous jet which can have important mixing, molecular stretching and bond-cleavage effects, as well as the more familiar cleaning phenomena. Finally, mention should be made of Rayleigh

streaming, which leads to cellular flow patterns with eddy lengths of $\frac{1}{4}\lambda$ induced by viscous effects in the boundary layer (Lighthill 1978*a*, *b*). This effect is often realized by banding of particles immersed in a planar acoustic field.

The next level of flow field which follows on theoretically from the discussion of Rayleigh streaming, is associated with microstreaming—the flow attributed to the oscillations of the bubble. Bubbles oscillating near boundaries can generate strong microstreaming flows, while, in the case of single-bubble sonoluminescence, microstreaming flows can be generated by the combined vigorous periodic volume change and translation. This may be further enhanced by the non-spherical collapse phase of the bubble, leading to a high-speed liquid jet and toroidal bubble generation (Longuet-Higgins 1997, 1998).

3. Non-spherical bubble dynamics

The spherically symmetric equations of motion normally used to model the large-amplitude oscillations of a bubble are those of a nonlinear oscillator. Prosperetti & Hao (this issue) discuss these models in the context of SCBL. The equations are derived for weakly compressible flows where the 'inner region' surrounding the bubble is effectively incompressible. This inner incompressible region around the bubble allows us to adapt the earlier studies in hydraulic cavitation to model some of the shorter-lifetime non-spherical bubble phenomena of acoustic cavitation.

The most extensively studied phenomenon in cavitation has been the incompressible-flow regime which leads to Laplace's equation for the potential ϕ:

$$\nabla^2\phi = 0. \tag{3.1}$$

Because the bubble shape is spatially and temporally unknown, the most successful numerical-solution technique has been based on a boundary integral method derived from Green's second theorem, whereby the potential ϕ may be represented as a surface integral over the bubble surface (and other boundaries) as follows:

$$c(\boldsymbol{p})\phi(\boldsymbol{p}) = \int_{\partial\Omega}\left(\frac{\partial\phi}{\partial n}(\boldsymbol{q})G(\boldsymbol{p},\boldsymbol{q}) - \phi(\boldsymbol{q})\frac{\partial G}{\partial n}(\boldsymbol{p},\boldsymbol{q})\right)\mathrm{d}\Omega_q. \tag{3.2}$$

Here G is a Green's function appropriate to the system under study, while $\boldsymbol{p}$ is the position vector of a point in the closure of the fluid domain Ω, and $\boldsymbol{q}$ is the position vector of a point on the boundaries of the domain, $\partial\Omega$ (such as the bubble surface). The coefficient $c(\boldsymbol{p})$ is defined to be $\frac{1}{2}$ if $\boldsymbol{p} \in \partial\Omega$ if $\partial\Omega$ is smooth, and unity if $\boldsymbol{p} \in \Omega \setminus \partial\Omega$. The solution procedure involves a discretization of the boundaries $\partial\Omega$ of the fluid domain Ω. Given the initial conditions of the position of any free surfaces and rigid boundaries together with the values of ϕ on the free surfaces and $\partial\phi/\partial n$ on the rigid boundaries, equation (3.2) may be solved numerically for the remaining unknowns, and most particularly for $\partial\phi/\partial n$ on the bubble surface. The sense of the normal vector to the surface, $\boldsymbol{n}$, is taken to be positive into the bubble interior. In order to advance the solution forward in time the kinematic and dynamic conditions are employed. Suppose that B is the surface of the bubble, then for $\boldsymbol{x} \in B$ we have

$$\frac{\mathrm{d}\boldsymbol{x}}{\mathrm{d}t} = \nabla\phi, \tag{3.3}$$

which can be used to update the position of the bubble surface, while the dynamic boundary condition,

$$\frac{\mathrm{d}\phi}{\mathrm{d}t} = \tfrac{1}{2}|\nabla\phi|^2 - \alpha(V_0/V)^\kappa - \delta^2(z - z_0) + \frac{K}{We} + 1, \tag{3.4}$$

can be used to update the potential. Note that these equations have been placed in non-dimensional form—lengths have been scaled with respect to the maximum bubble radius R_m, time with respect to $R_\mathrm{m}\sqrt{\rho/\Delta p}$ and pressure with respect to $\Delta p = p_\infty - p_\mathrm{V}$. Here p_∞ is the hydrostatic pressure at the depth of the bubble's inception, p_V is the liquid vapour pressure and ρ is the density. The terms on the right-hand side of equation (3.4) are physically associated with, respectively: (i) fluid inertia; (ii) adiabatic compression of the gaseous bubble; (iii) buoyancy; and (iv) surface tension. Viscous surface stresses have not been included in these studies. The dimensionless terms in this expression are as follows: $\alpha = p_0/\Delta p$, where p_0 is the pressure due to the non-condensible contents of the bubble, κ is the polytropic index of the gas in the bubble, $\delta = \sqrt{\rho g R_\mathrm{m}/\Delta p}$ is the dimensionless buoyancy parameter, K is the curvature of the bubble surface and $We = R_\mathrm{m}\Delta p/\sigma$ is the Weber number where σ is the surface tension. More details on this aspect may be found in Blake *et al.* (1986, 1987), Blake & Gibson (1987) and Blake *et al.* (1997).

Bubbles are subject to the hydrodynamic interaction with other bubbles, rigid boundaries, free surfaces, gravity, acoustic pressures, and in some cases shock waves, that lead to asymmetries. In many circumstances this leads to the presence of a liquid jet that penetrates the interior of the bubble, on occasions at extremely high velocities (50 m s^{-1}–4 km s^{-1}), with the higher velocities clearly violating the incompressibility assumptions. These jets impact on the far side of the bubble leading to a toroidal bubble geometry. The previous numerical technique needs to be modified to allow the study to move into a multiply connected flow domain. Connectivity is restored by means of a fictitious 'cut' across the liquid jet, leading to a modified boundary integral equation (Best 1993):

$$c(\boldsymbol{p})\phi(\boldsymbol{p}) = \int_{\partial\Omega}\left(\frac{\partial\phi}{\partial n}(\boldsymbol{q})G(\boldsymbol{p},\boldsymbol{q}) - \phi(\boldsymbol{q})\frac{\partial G}{\partial n}(\boldsymbol{p},\boldsymbol{q})\right)\mathrm{d}\Omega_q - \Delta\phi\int_T \frac{\partial G}{\partial n_+}(\boldsymbol{p},\boldsymbol{q})\,\mathrm{d}\Omega_q. \tag{3.5}$$

Integration over the cut T takes account of any circulation introduced at the jet impact by allowing a jump in ϕ values with $\Delta\phi = \phi_+ - \phi_-$, where the $\pm$ identifies the upper and lower surfaces. The central concept of the theory depends on impact at a point with no resulting generation of a vortex sheet. This is consistent with the original mathematical model, which does not allow any mechanism for dissipation of energy, and with recent experimental studies of droplet impact (Cresswell & Morton 1995).

We illustrate this approach by considering collapsing gas bubbles near a rigid boundary for different stand-off values $\gamma = h/R_\mathrm{m}$, where h is the dimensional stand-off distance and R_m is the maximum bubble radius. In these cases, which are chosen to correspond to laser-generated bubbles with $R_\mathrm{m} \simeq 1.3$ mm, the Weber number is found to be approximately equal to 1.7×10^3 and so the surface tension term K/We is neglected in these calculations, as is buoyancy. Figure 1 shows the evolution of bubble shapes over several time periods for $\gamma = 0.98$ (figure 1*a*) and $\gamma = 5.2$ (figure 1*b*). It is interesting to compare the velocities of the 'north pole' of adiabatic gas bubbles

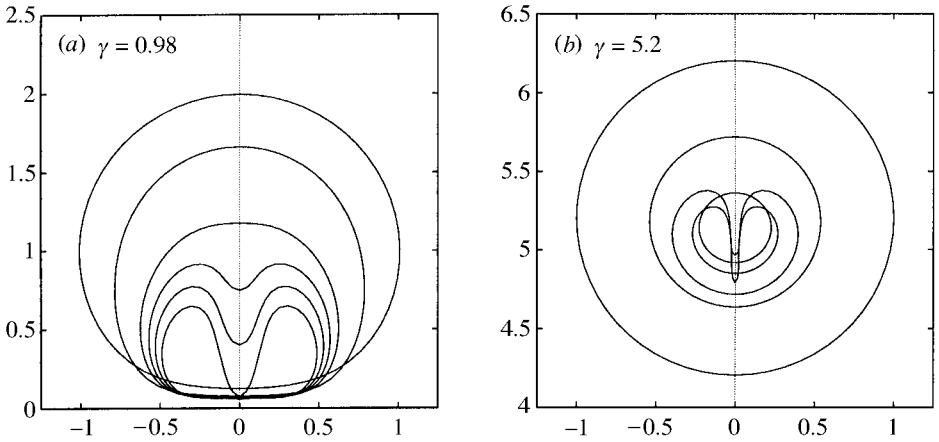

Figure 1. Gas bubble collapse near a rigid boundary.

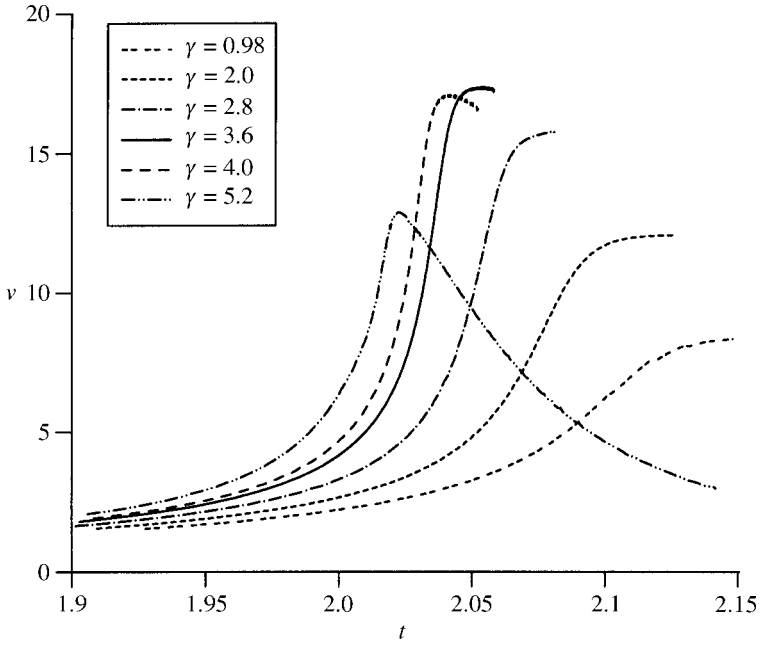

Figure 2. Jet velocities during gas bubble collapse for various values of γ.

(pressure in the bubble interior, $p_{\mathrm{i}} = p_{\mathrm{V}} + p_0(V_0/V)^{\kappa}$) near a rigid boundary for different dimensionless stand-off distances γ (see figure 2). The important observation is that the gas bubble has a peak jet velocity which is obtained at a certain value of γ ($\gamma \simeq 3.6$) for specified physical parameters, with our calculations being illustrated here for one set ($\alpha = 100$, $\kappa = 1.4$, $We \to \infty$, $\delta = 0$ (figure 2)) to show the qualitative behaviour. This peak velocity is attained when jet impact occurs at the 'south pole' at minimum bubble volume. Jet velocities are lower for impact before minimum volume and likewise for impact after the minimum volume has been reached, which ultimately leads to no impact at all, but rather to rebound of the bubble. Bubble shapes for the special case of maximum jet velocity at minimum volume are shown in the toroidal

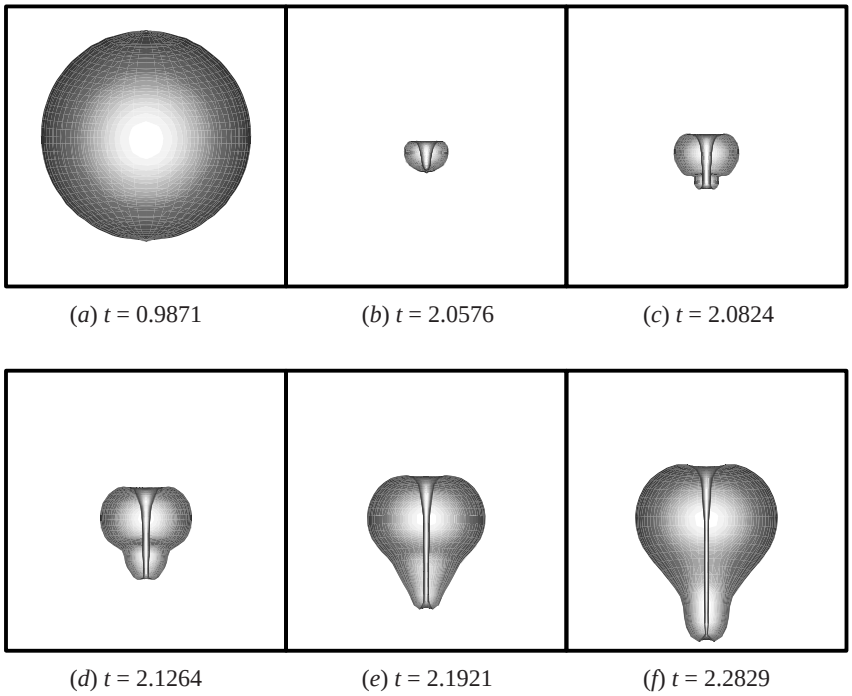

Figure 3. A rendered half-section of a collapsing cavitation bubble at $\gamma = 3.6$, showing the very fine and thinning jet as the bubble rebounds. Jet impact occurs at minimum volume. (*a*) Bubble at maximum radius.

bubble geometry both before and after impact with the thin central core of liquid (figure 3). Examples of this are also illustrated in Ohl *et al*. (this issue). Features of this calculation that are of importance to sonophysicists and sonochemists are the high strain rates that will occur in the liquid in the region of inflow of the jet at the 'north pole' and immediately after jet impact at the 'south pole'. This may provide sites for cleavage of macromolecules. Immediately after jet impact, the high pressure on impact forces the fluid to the side, partly splashing back into the bubble, which is apparent in figure 3*c*. This phenomenon is also clearly present later, in figure 9. In addition the toroidal-bubble behaviour will enhance mixing and hence reaction rates, especially if reactive chemical species are nearby. High temperatures will also occur inside the bubble due to adiabatic heating, providing a reactive chemical environment for the thin thread of liquid penetrating the bubble interior.

4. Bubble behaviour near an oscillating boundary

One of the most striking pictures that has occurred in the acoustic cavitation literature has been the beautifully clear picture by Crum (figure 4) (see Prosperetti 1984; Suslick 1989) of a sharp clean jet penetrating a cavitation bubble in the direction of the oscillating table (a relatively low-frequency paint mixer). If the video from which this picture has been taken is studied in greater detail, two further features are apparent. First, the remarkable stability of the bubble motion—the presumably toroidal bubble regenerates as a simply connected bubble; i.e. it expands to maximum volume

Figure 4. Crum's photograph of jet formation during bubble collapse

ready to collapse again with almost identical jet behaviour. However, occasionally a small bubble is shed from the upper surface. This is not entirely unexpected because similar phenomena are known to exist when a cavitation bubble grows and collapses in a stagnation-point flow (Blake *et al*. 1986; Robinson & Blake 1994).

Furthermore, a whole range of oscillatory bubble behaviour and bubble shapes were obtained, and reported in Crum's original (1979) paper. Here we briefly develop theory to enable us to study the observations in greater detail.

It is relatively straightforward to incorporate the oscillating table into the previous theory for an incompressible bubble by using a modified gravitational term $g' = g - \omega^2 a \sin \omega t$ associated with a sinusoidal displacement of the table, given by $a \sin \omega t$. The pressure field measured by Crum (1979) confirms this approach as a valid approximation. The term for $\mathrm{d}\phi/\mathrm{d}t$ in (3.4) in dimensional terms becomes

$$\frac{\mathrm{d}\phi}{\mathrm{d}t} = \tfrac{1}{2}|\nabla\phi|^2 + \frac{1}{\rho}\left(p_\infty - p_0\left(\frac{V_0}{V}\right)^\kappa + \sigma\left(\frac{1}{R_1} + \frac{1}{R_2}\right)\right) + (g - \omega^2 a \sin\omega t)(z - H). \tag{4.1}$$

In this case we will scale time with respect to the driving frequency of the oscillating table, leading to the following dimensionless parameters:

$$\mathcal{P} = \frac{p_\infty}{\rho\omega^2 R_0^2}, \quad \alpha = \frac{p_0}{p_\infty}, \quad We^* = \frac{R_0 p_0}{\sigma},$$
$$\beta = \frac{a}{R_0}, \quad g^* = \frac{g}{\omega^2 R_0}, \quad \gamma = \frac{H}{R_0},$$

which in turn lead to the following dimensionless form:

$$\frac{\mathrm{d}\phi}{\mathrm{d}t} = \mathcal{P}\left[1 - \alpha\left(\frac{V_0}{V}\right)^\kappa + \frac{1}{We^*}\left(\frac{1}{R_1} + \frac{1}{R_2}\right)\right] + (g^* - \beta \sin 2\pi t)(z^* - \gamma) + \tfrac{1}{2}|\nabla\phi|^2. \tag{4.2}$$

Some data on parameters are available from Crum (1979), but for others we have had to estimate them. Examples for bubbles near a rigid boundary are illustrated in figures 5 and 6.

Figure 5 provides diagrams that yield similar bubble shapes to those associated with the bubble in figure 4, i.e. a flat oblate-shaped bubble with a 'bump' on the upper surface that becomes a liquid jet penetrating the interior of the bubble. A slight change in the parameters would lead to a small bubble being ejected at the stage between times 1.88 and 1.91 in figure 5. Figure 6 shows a more elongated

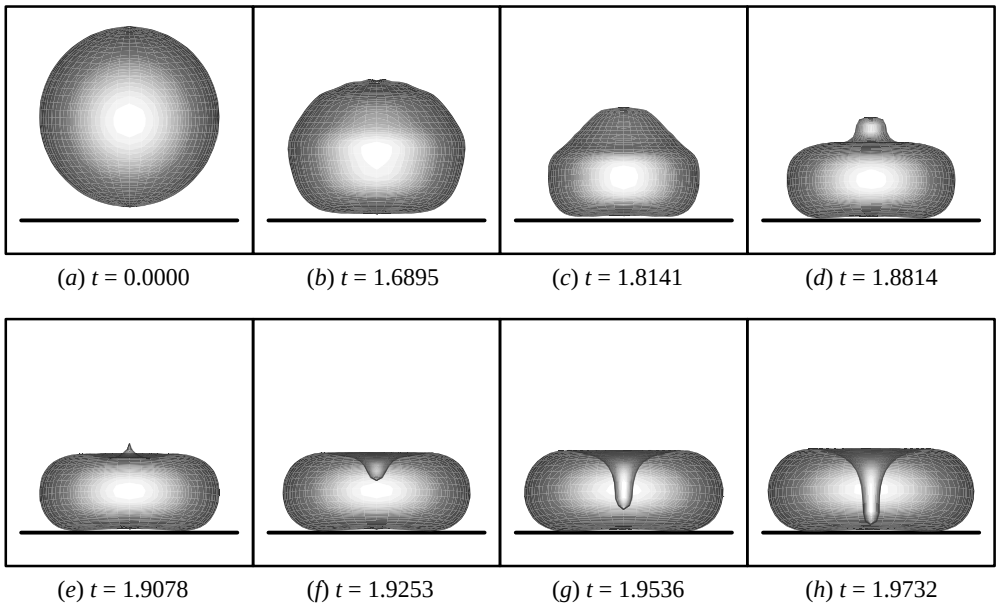

Figure 5. Oscillating boundary BIM calculations: stand-off 1.15; amplitude of oscillation 2 mm.

version of the bubble shape for a greater amplitude of oscillation and slightly smaller stand-off.

5. Bubble interactions and bubble clouds

Bubble interactions within clouds or assemblies exhibit a variety of interesting behaviours governed by primary and secondary Bjerknes forces. In an acoustic standing wave, pressure gradients lead to migration of bubbles towards either the pressure node or antinode—a bubble-size-dependent phenomenon. Depending on the respective phase of their oscillations, the rate of attraction or repulsion is enhanced considerably. Studies of pairs or clouds of bubbles in an acoustic field are limited, with most of our knowledge in this area being gained from hydraulic cavitation or from studies of laser-generated cavities. Calculations indicate that the outer shell of bubbles is shielded by the central bubbles, and a layered collapse ensues. The generation of extremely high pressures near to the 'centre' is a consequence, and this is believed to be a mechanism for substantial noise generation from within the cloud (van Wijngaarden 1994).

Generally, in an inviscid flow the spherical assumption for the bubble can be an adequate representation of the surface if the fluid flow pressures (inertia) are much smaller than the surface pressure composed of: (1) a restoring pressure due to surface tension; or (2) a high internal bubble pressure. When the first condition is dominant, volume fluctuations are small and have a negligible effect on the bubble dynamics. For the study of such flows, force-balance methods have been extremely successful at predicting the transient dynamics of the spherical bubbles. For example, Kok (1993) analysed the motion of a pair of equiradii rising gas bubbles. For larger assemblies, Sangani & Didwania (1993*a*, *b*) showed that the interactions result in the formation

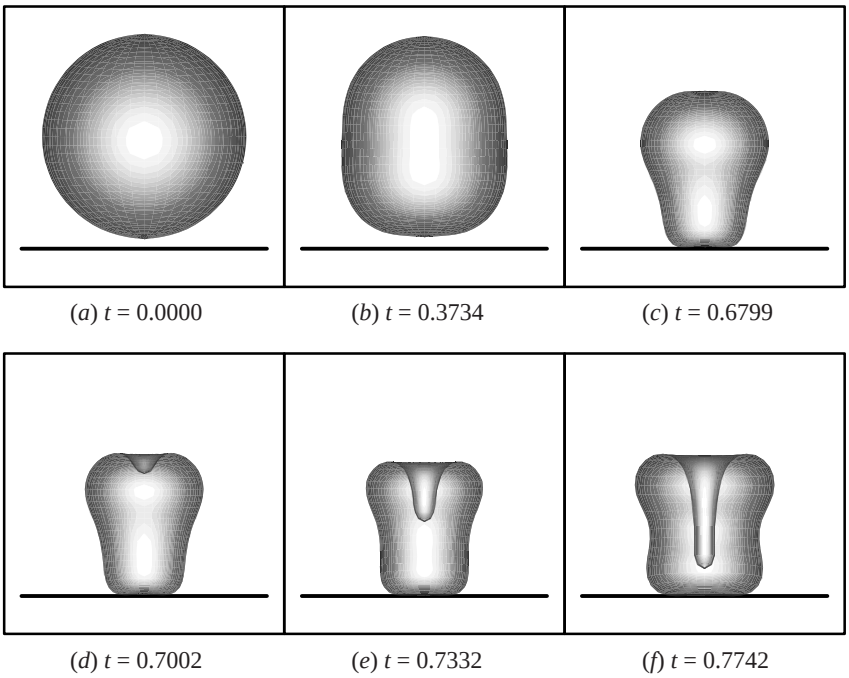

Figure 6. Oscillating boundary BIM calculations: stand-off 1.1; amplitude of oscillation 3 mm.

of clusters positioned broadside to the direction of the (mean) flow. It is observed that under the second condition the spherical approximation fails during only the last stages of collapse, over only about 3% of the bubble lifetime.

As before, we consider a fluid that is irrotational, unsteady and inviscid. The flow shall be taken to be composed solely of an arbitrary number of bubbles, but is otherwise unbounded. Consider the surface of bubble j. Without loss of generality we may represent the normal surface velocity in the following form:

$$\boldsymbol{u}_j \cdot \boldsymbol{n} = U_j^k \psi_{jk}. \tag{5.1}$$

Here U_j^k is used to represent the components of the surface velocity at the surface of bubble j, ψ_{jk} is the amplitude of the corresponding surface mode in an analytical representation and the summation over k is implied. In a similar manner, a general solution to the boundary-value problem represented by equations (3.1), (3.3) and (3.4) can be constructed from a set of coefficients, ϕ^k, and spatial functions, χ_k:

$$\phi = \phi^k \chi_k. \tag{5.2}$$

In practice, a multipole solution is adopted for these spatial functions. It follows directly from the linearity of Laplace's equation and (5.1) that this solution for ϕ can be expressed in the Kirchhoff form

$$\phi = D_k^l \chi_l U_j^k, \tag{5.3}$$

where the coefficients D_k^l are dependent solely on the flow configuration, and again all summations are implied. To construct these unknown coefficients, we have used a variational principle applied by Miles (1976). Miles showed that minimization of the

fluid kinetic energy when expressed in suitable integral form leads to a set of coupled equations

$$D_k^l \phi_k = \sum_j E_{jk}^l U_j^k, \tag{5.4}$$

with the components of D_k^l, E_{jk}^l given by

$$D_k^l = \int_{\partial\Omega} \chi_l \frac{\partial \chi_k}{\partial n}\,\mathrm{d}S, \quad E_{jk}^l = \int_{S_j} \chi_l \psi_{jk}\,\mathrm{d}S. \tag{5.5}$$

Here $\partial\Omega = \sum_j S_j$ denotes the collective surfaces. Expression (5.4) may be cast into matrix form, and, if the surface variation is prescribed, inverting the resulting matrix equation provides us with the unknowns, ϕ_k. In general the system is either exactly prescribed or overprescribed depending on how many more potential modes than surface modes are chosen.

The solution method for the flow dynamics is based on a weighted residual formulation, in conjunction with Bernoulli's equation for the fluid pressure and continuity of the stress normal to the gaseous boundary. Under the stated assumptions of potential flow, continuity of stress provides the following dynamic boundary condition at the surface of each bubble, j:

$$\frac{\mathrm{d}\phi}{\mathrm{d}t} = \tfrac{1}{2}|\nabla\phi|^2 + \frac{1}{\rho}(p_\infty - p_j + \sigma\nabla\cdot\boldsymbol{n}) + g(z_j - H_j), \tag{5.6}$$

where p_j is the pressure due to any gaseous contents, σ is the surface tension, g is the gravitational constant and $(z_j - H_j)$ is the surface depth. Multiplying by a weighting function $\mathcal{W}$ and integrating over the collective flow boundaries, $\partial\Omega$, we obtain

$$\dot{\phi}_k \int_{\partial\Omega} \mathcal{W}\chi_k\,\mathrm{d}S = \sum_j \int_{S_j} \mathcal{W}\left[\frac{1}{\rho}(p - -p_j + \sigma\nabla\cdot\boldsymbol{n}) + g(z_j - H_j)\right]_{\boldsymbol{\Phi}} \mathrm{d}S. \tag{5.7}$$

Here the bracketed term is evaluated at constant $\boldsymbol{\Phi}$. We can construct a coupled set of differential equations for the rate of change of the velocity potential, which when cast into matrix form yields $\dot{\phi}_k$ on inversion. The choice of $\mathcal{W} = \partial\chi_j/\partial n$ was made from a practical point of view since the resulting integral quantities arise in the described method of solution for ϕ (see (5.5)). This equation, along with (5.4), is non-dimensionalized as in § 3, and subject to appropriate initial conditions, they are solved concurrently using a fourth-order time-stepping scheme. This provides a simple algorithm to step the surface forward in time. For the results presented, we have chosen a multipole representation for the velocity potential and a low-order spherical-harmonic description of each bubble surface, S_j:

$$S_j = s_j - R_j = 0, \tag{5.8}$$

$$R_j = \sum_{n=0}^{\infty}\sum_{m=0}^{n} a_{nm,j}\cos(\varpi_j)P_{nm}(\theta_j) + \tilde{a}_{nm,j}\sin(m\varpi_j)P_{nm}(\theta_j). \tag{5.9}$$

Here $a_{nm,j}, \tilde{a}_{nm,j}$ denote the amplitudes of the surface modes, P_{nm} the Legendre polynomials and s_j, θ_j, ϖ_j are the radial, polar and azimuthal coordinates in a spherical-coordinate system local to each bubble. In practice the series is truncated appropriately.

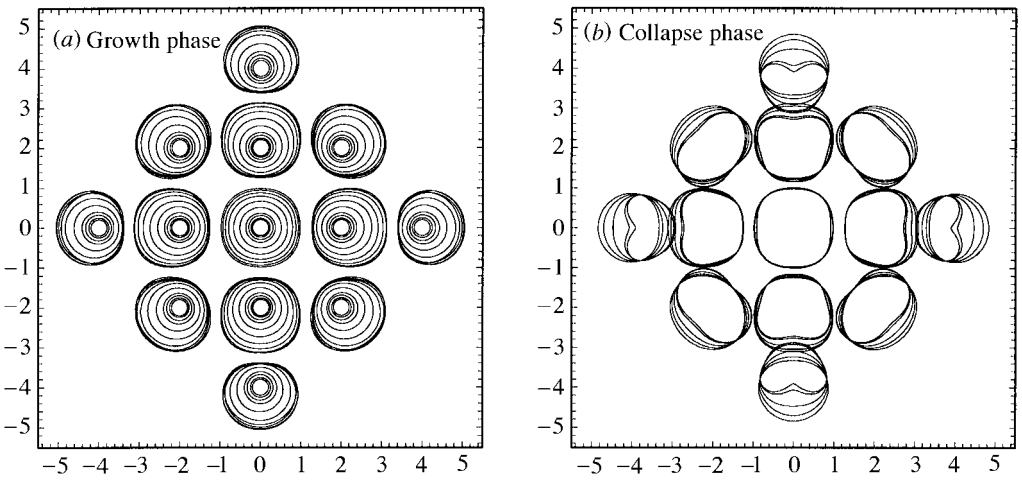

Figure 7. Growth and collapse phase for a 13 bubble array having an initial radius $0.2R_{\mathrm{m}} = 0.2 \times 10^{-4}$ m, $p_{\mathrm{g}} = 25.7p_{\infty}$.

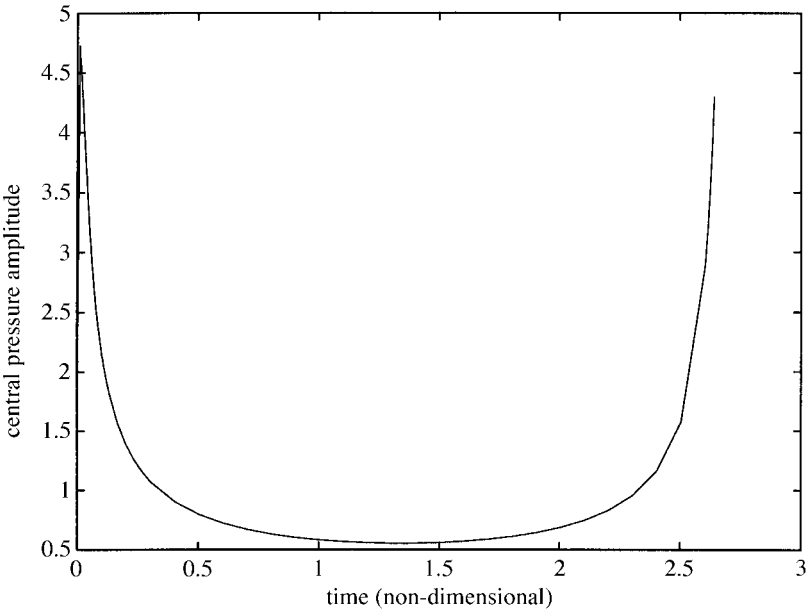

Figure 8. Variation in peak pressure for a cubic array.

When such assemblies are subjected to a sudden pressure drop within the ambient fluid (or equivalently undergo explosive growth), the simulations highlight the fact that a staggered collapse ensues. For a dense cloud of bubbles of similar size, the collapse is observed to propagate inwards through the fluid. An example of such a simulation performed on bubbles placed spatially in an array within some given unit cell is demonstrated for 13 bubbles in figure 7.

We notice that the collapse propagates from the outer bubbles inwards, but the central bubble, not having quite attained a maximum radius, is to a large extent unaffected by this early stage of collapse. These numerical results appear to predict

the correct overall collapse behaviour up to the point where surface jets develop. Unfortunately it is not possible to resolve the collapse beyond these initial jet profiles, owing to the inherent instability of multipole solutions. This is of course a region of primary interest since the maximum fluid pressures occur just after the preliminary jet–surface impact.

The growth and collapse of more sparse arrays exhibit a similar behaviour with the jets again directed towards the array centre. For a sparse cubic array of size $10R_{\mathrm{m}} \times 10R_{\mathrm{m}}$, the temporal variation in the central pressure, shown in figure 8, suggests that during such a collapse extremely large pressures are generated within the fluid. However, as one would expect, larger, more dilute, assemblies exhibit no general direction for the collapse. Furthermore, smaller bubbles may reach their maximum volume first, with the consequence that a number of indistinct collapses will occur or the collapse may propagate outwards away from the centre.

6. Jet impact and damage to boundaries

One of the well-known features of hydraulic cavitation is the pitting of propeller and impeller blades (see, for example, Burrill 1951; Leighton 1994; Trevena 1987). In acoustic cavitation this phenomenon can be exploited to clean surfaces. A very simple illustration of this phenomenon is to place a piece of aluminium foil in an acoustic bath for a few seconds and observe the many punctures in the sheet on removal. This technique can be exploited during oxidation processes to keep reaction surfaces clean. This may also be the mechanism for enhanced performance of tanning in the leather industry.

An understanding of the fluid mechanisms of jet impact on a rigid boundary has received a number of careful studies on both the experimental and theoretical sides. However, they would appear to be much more complex phenomena than simply jet impact, as there are often the additional features of shock waves and high pressures (and possibly temperatures) associated with the compression of the gaseous content of the bubble.

Tomita & Shima (1986) provided a thorough and detailed analysis of the growth and collapse of a laser-generated bubble near a rigid boundary. They found that damage was associated with both shock waves and also the impact between the liquid drawn in from the far-field by the collapsing bubble with the outward-flowing liquid associated with the after effects of the liquid jet impacting against the boundary. Surprisingly, the peak pressures were not associated with jet impact, but were attributed to the impact associated with the subsequent collision of liquid masses and shock waves. Analysis of stress waves in the solid boundary confirmed the occurrence of these events. Philipp & Lauterborn (1997, 1998) have more recently exploited very high-speed camera observations of the jet-impact process, noting the development of shock waves at differing locations associated with separate events. This work is reported in greater detail in Ohl *et al.* (this issue).

Theoretical studies of this phenomenon are limited to the incompressible regime, but are nevertheless revealing with regard to some of the characteristics of fluid behaviour immediately following jet impact. The studies of Tong *et al.* (1999) and Blake *et al.* (1998) reveal the significance of the 'splash' in generating high pressures in the incompressible regime (figure 9). The splash is associated with the collision of the outer inflow, due to bubble collapse, with the inner flow, associated with

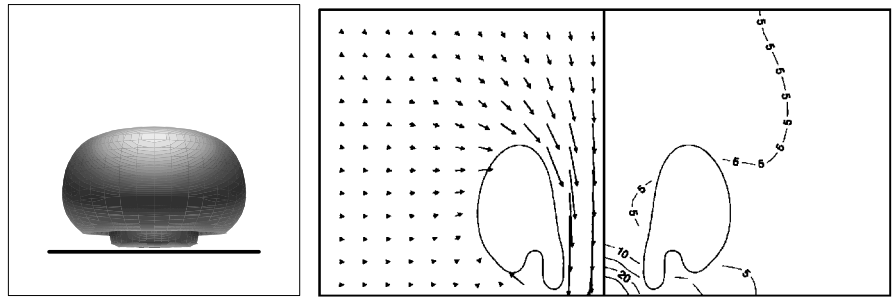

(*a*) $t = 2.2798$

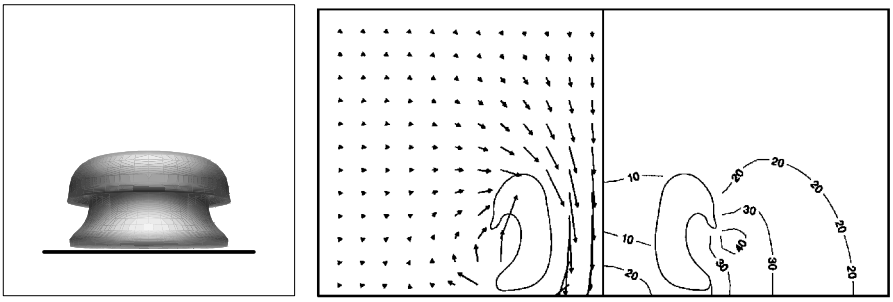

(*b*) $t = 2.3146$

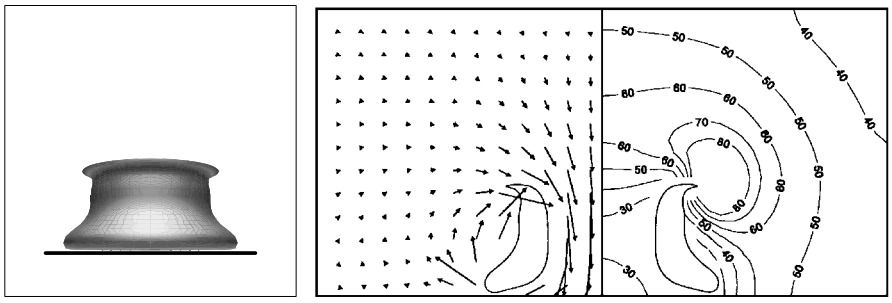

(*c*) $t = 2.3271$

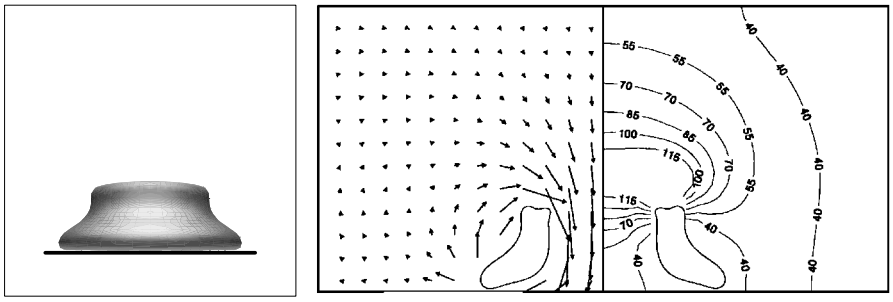

(*d*) $t = 2.3341$

Figure 9. Rendered bubble views, together with cross-sectional velocity vectors and pressure fields for the toroidal stage of bubble collapse near a rigid boundary for $\gamma = 0.98$, $\alpha = 100$, $\kappa = 1.4$. The arrows indicate the relative magnitude and absolute direction of the fluid velocities and the numbers refer to the dimensionless pressures along the contours.

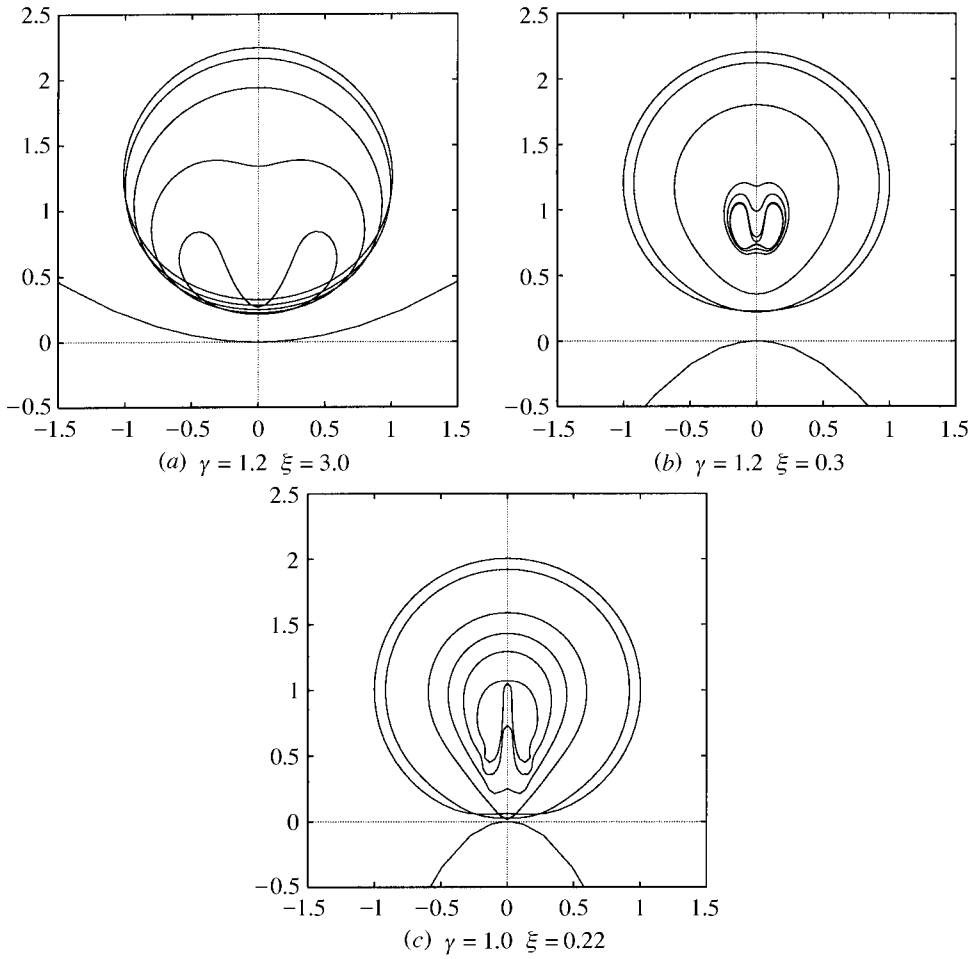

Figure 10. Calculations of bubble collapse near a curved rigid boundary: $\alpha = 100$, $\kappa = 1.4$.

the outward jet flow along the rigid boundary. This leads to a stagnation flow on a circular ring which, when coupled with the higher internal gas pressure, gives a larger pressure on the boundary than that associated with jet impact (figures 9*b*, *c*). Later still, shock waves may yield higher pressures as the bubble rebounds on reaching minimum volume. An interesting characteristic of these experimental studies is the observation of pitting in a circular zone with a radius in the range of 0.6–0.8 of the maximum bubble radius; a figure which is consistent with the incompressible-flow analysis. More recently, Philipp & Lauterborn (1998) have observed that laser-generated single-cavitation bubbles collapsing near an aluminium surface give rise to pitting at a point below the bubble centre for $1.7 < \gamma < 2$, while for $\gamma \leqslant 1.7$, when the bubble is toroidal, the pitting forms a ring below the bubble.

7. Behaviour near rough surfaces

Cavitation bubbles often cause mechanical damage to a surface, thus leading to the study of the behaviour of bubbles near rough surfaces. How do rough surfaces

influence the behaviour of the bubbles as well as serving as a nucleation site for the development of further bubbles? There have been observations which suggest that the rough surfaces, which are formed as a result of surface damage, accelerate and promote cavitation damage still further. There has been little experimentation on the motion of cavitation bubbles near rough surfaces, but we do report on some of the recent experimental studies by Tomita *et al*. (1998). These concern the growth and collapse of cavitation bubbles near a curved rigid boundary—that is to say that this study is relevant where the sizes of individual bubbles are roughly comparable to the scale of the surface roughness (the effect of surface distortion on the motion of bubbles is enhanced in this case). Eick (1992), meanwhile, has performed calculations on the motion of a bubble in a conical hollow and also in the vicinity of a wavy rigid surface, where the amplitude of the waves in the surface is comparable to the size of the bubble.

Tomita *et al*. (1998, 1999) used high-speed photography to observe the evolution of cavitation bubbles near a known curved rigid boundary. These bubbles are produced using a standard technique for achieving high-energy concentrations—a laser-focusing technique described by Lauterborn (1972). Boundary integral-method calculations have been performed to mimic these experiments, producing good comparison with experiment (see figure 10). The rigid boundary is defined in cylindrical polar coordinates as

$$f(r,z) = (r^2 + (\gamma - z)^2)^{1/2}(\xi^2(z + \xi\gamma) + (1 - \xi^2)(r^2 + (z + \xi\gamma)^2)^{1/2}) - (\gamma - z)(r^2 + (z + \xi\gamma)^2)^{1/2} = 0. \quad (7.1)$$

The curvature is determined by the parameter ξ, where $\xi < 1.0$ gives a convex shape and $\xi > 1.0$ gives a concave shape.

In figure 10*a* a bubble is shown collapsing in a concave region with a liquid jet directed towards the wall. Figure 10*b* shows the development of a jet from both ends of the bubble, leading to an internal impact within the bubble. Figure 10*c*, for the case of a more needle-like roughness, records a high-speed jet directed away from the boundary. This is due to the bubble 'hanging-up' on the projection, leading to high curvature in the lower bubble surface and thence a rapid collapse and subsequent jet from this side. Whether this interesting behaviour near rough surfaces may be exploited could be the subject of further theoretical and experimental studies.

8. Conclusions

Non-spherical bubble behaviour is likely to be the norm in nearly all acoustic cavitation studies and warrants far more attention than it has received to date. Interactions with the driving acoustic pressure field, boundaries, other bubbles and buoyancy forces will all lead to asymmetric bubble behaviour. The consequences are: high velocities, often in the form of a high-speed jet; higher pressures; zones of impact; high strain rates; and better mixing. This improved understanding of the fluid dynamics of these phenomena should provide a greater insight into areas of application in sonophysics, sonochemistry, medicine and in industry.

Funding for this research programme has been provided by the EPSRC Mathematics Programme and DERA/MoD, which is gratefully acknowledged.

References

Best, J. P. 1993 The formation of toroidal bubbles upon the collapse of transient cavities. *J. Fluid Mech.* **251**, 79–107.

Blake, J. R. 1971 A note on the image system for a stokeslet near a no-slip boundary. *Proc. Camb. Phil. Soc.* **70**, 303–310.

Blake, J. R. & Gibson, D. C. 1987 Cavitation bubbles near boundaries. *A. Rev. Fluid Mech.* **19**, 99–123.

Blake, J. R., Taib, B. B. & Doherty, G. 1986 Transient cavities near boundaries. Part 1. Rigid boundary. *J. Fluid Mech.* **170**, 479–497.

Blake, J. R., Taib, B. B. & Doherty, G. 1987 Transient cavities near boundaries. Part 2. Free surface. *J. Fluid Mech.* **181**, 197–212.

Blake, J. R., Hooton, M. C., Robinson, P. B. & Tong, R. P. 1997 Collapsing cavities, toroidal bubbles and jet impact. *Phil. Trans. R. Soc. Lond.* A **355**, 537–550.

Blake, J. R., Tomita, Y. & Tong, R. P. 1998 The art, craft and science of modelling jet impact in a collapsing cavitation bubble. *Appl. Sci. Res.* **58**, 77–90.

Burrill, L. C. 1951 Sir Charles Parsons and cavitation. *Trans. Inst. Marine Engrs* **63**, 149–167.

Cresswell, R. W. & Morton, B. R. 1995 Drop-formed vortex rings—The generation of vorticity. *Phys. Fluids* **7**, 1363–1370.

Crum, L. A. 1979 Surface oscillations and jet development in pulsating bubbles. *J. Physique* **40**, C8-285–C8-288.

Eick, I. 1992 Experimentelle und numerische Untersuchungen zur Dynamik sphärischer und asphärischer Kavitationsblasen. PhD thesis, Darmstadt.

Gilmore, F. R. 1952 The collapse and growth of a spherical bubble in a viscous compressible liquid. Hydrodynamics laboratory report no. 26-4. California Institute of Technology, Pasadena, USA.

Keller, J. B. & Kolodner, I. T. 1956 Damping of underwater explosion bubble oscillations. *J. Appl. Phys.* **27**, 1152–1161.

Kok, J. B. W. 1993 Dynamics of a pair of gas bubbles moving through liquid. *Eur. J. Mech.* B (*Fluids*) **12**, 515–540.

Lauterborn, W. 1972 High-speed photography of laser-induced breakdown in liquids. *Appl. Phys. Lett.* **21**, 27–29.

Leighton, T. G. 1994 *The acoustic bubble*. London: Academic.

Lighthill, J. 1978*a* Acoustic streaming. *J. Sound Vibrat.* **61**, 391–418.

Lighthill, J. 1978*b* *Waves in fluids*. Cambridge University Press.

Lohse, D. 1998 Lasers blow a bigger bubble. *Nature* **392**, 21.

Longuet-Higgins, M. S. 1997 Particle drift near an oscillating bubble. *Proc. R. Soc. Lond.* A **453**, 1551–1568.

Longuet-Higgins, M. S. 1998 Viscous streaming from an oscillating spherical bubble. *Proc. R. Soc. Lond.* A **454**, 725–742.

Miles, J. W. 1976 Nonlinear surface waves in closed basins. *J. Fluid Mech.* **75**, 418–448.

Moss, W. C., Clarke, D. B. White, J. W. & Young, D. A. 1994 Hydrodynamic simulations of bubble collapse and picosecond sonoluminescence. *Phys. Fluids* A **6**, 2979–2985.

Ohl, C. D., Lindau, O. & Lauterborn, W. 1998 Luminescence from spherically and aspherically collapsing laser induced bubbles. *Phys. Rev. Lett.* **80**, 393–396.

Philipp, A. & Lauterborn, W. 1997 Damage of solid surfaces by single laser-produced cavitation bubbles. *Acustica* **83**, 223–227.

Philipp, A. & Lauterborn, W. 1998 Cavitation erosion by single laser-produced bubbles. *J. Fluid Mech.* **361**, 75–116.

Prosperetti, A. 1984 Bubble phenomena in sound fields. Part 2. *Ultrasonics* **22**, 115–124.

Prosperetti, A. 1997 A new mechanism for sonoluminescence. *J. Acoust. Soc. Am.* **101**, 2003–2007.

Riley, N. 1998 Acoustic streaming. *Theoret. Comput. Fluid Dynam.* **10**, 349–356.

Robinson, P. B. & Blake, J. R. 1994 Dynamics of cavitation bubble interactions. In *Bubble dynamics and interface phenomena* (ed. J. R. Blake, J. M. Boulton-Stone & N. H. Thomas), pp. 55–64. Dordrecht: Kluwer.

Sangani, A. S. & Didwania, A. K. 1993*a* Dispersed-phase stress tensor in flows of bubbly liquids at large Reynolds numbers. *J. Fluid Mech.* **248**, 27–54.

Sangani, A. S. & Didwania, A. K. 1993*b* Dynamic simulations of flows of bubbly liquids at large Reynolds numbers. *J. Fluid Mech.* **250**, 307–337.

Suslick, K. S. 1989 The chemical effects of ultrasound. *Scientific American* **260**, 80–86.

Tomita, Y. & Shima, A. 1986 Mechanisms of impulsive pressure generation and damage pit formation by bubble collapse. *J. Fluid Mech.* **169**, 535–564.

Tomita, Y., Blake, J. R. & Robinson, P. B. 1998 Interaction of a cavitation bubble with a curved rigid boundary. In *Proc. 3rd Int. Symp. on Cavitation, Grenoble, France.*

Tomita, Y., Blake, J. R., Tong, R. P. & Robinson, P. B. 1999 Growth and collapse of cavitation bubbles near a curved rigid boundary. (In preparation.)

Tong, R. P., Schiffers, W. P., Shaw, S. J., Blake, J. R. & Emmony, D. C. 1999 The role of 'splashing' in the collapse of a laser-generated cavity near a rigid boundary. *J. Fluid Mech.* **380**, 339–361.

Trevena, D. H. 1987 *Cavitation and tension in liquids.* Bristol: IOP Publishing.

van Wijngaarden, L. 1994 Bubble dynamics and the sound emitted by cavitation. In *Bubble dynamics and interface phenomena* (ed. J. R. Blake, J. M. Boulton-Stone & N. H. Thomas), pp. 181–193. Dordrecht: Kluwer.

PHILOSOPHICAL TRANSACTIONS OF THE ROYAL SOCIETY A MATHEMATICAL, PHYSICAL & ENGINEERING SCIENCES